Orientation of Drawn Nafion at Molecular and Mesoscopic Scales

P. C. van der Heijden, L. Rubatat, and O. Diat*

Département de Recherche Fondamentale sur la Matière Condensée, SI3M/Groupe Polymères Conducteurs Ioniques, CEA Grenoble, 17 rue des Martyrs, 38054, Grenoble Cedex 9, France

Received October 31, 2003; Revised Manuscript Received April 30, 2004

ABSTRACT: The structural orientation in Nafion films in an ambient environment and under stretching is analyzed using small/wide-angle X-ray scattering. On the basis of the absolute values of Hermans' orientation factor, we characterize the structural anisotropy at different length scales (between angstroms and several hundreds of angstroms) in agreement with a previously proposed fibrillar model of the Nafion membrane. Bundles of elongated polymeric aggregates orient at small draw ratios, together with an orientation of the aggregates within such a bundle. The crystal structure of this semicrystalline polymer is analyzed, and we show that the crystallinity of the Nafion film does not change as a function of the draw ratio.

Introduction

Nafion is a frequently used polymer for proton exchange membrane fuel cells (PEMFC) because of its good chemical, mechanical, and proton-transport properties. Nowadays, it is the reference polymer in the research to new polymeric materials for PEM fuel cells. Since its development in the mid-1960s, much research has been carried out to understand the structure of Nafion. Many different experimental techniques have been used, especially scattering techniques, in which the correlation lengths are determined. For an overview of experimental results and models, see for example refs 1−3. Experiments in the very diluted regime show the existence of aggregates of Nafion with the ionic groups at the surface,[1,4] whereas in the concentrated regime water pools with the ionic groups in a polytetrafluoroethylene matrix were proposed.[5] The transition between the concentrated and diluted regimes is still a point of debate.[6] To match the results between the diluted and concentrated regime, recent work proposes the existence of elongated polymeric aggregates in the concentrated region[7,8] The typical diameter of such an aggregate is 3−4 nm, and it is furthermore proposed that these aggregates are entangled with an orientation correlation length on the order of 100 nm.[9]

If Nafion films indeed consist of a collection of asymmetric polymer aggregates, it should be possible to orient them upon drawing, and this should result in differences in the properties of a Nafion film. In our previous paper,[10] birefringence results were presented and discussed, and it appeared that the birefringence was caused by orientation of polymer chains. Furthermore, we showed that the initial orientation, the preorientation, which stems from the manufacturing procedure, is reversible.

Already in the pioneering work of Gierke et al.,[5] SAXS experiments were carried out on drawn Nafion films. After this, a number of other SAXS experiments on deformed Nafion have been carried out[11−15] to study the effect of stretching on the distribution of the water pools in the polymer matrix. On one hand, Londono et al.[14] showed that the intensity distribution of the ionomer peak is anisotropic in the plane of the film parallel to the draw direction, whereas it is isotropic in the plane perpendicular to the draw direction. They concluded from their results that the Nafion structure consists of coalesced water pools, which form cylindrical or lamellar domains. On the other hand, Elliot et al.[13] discussed SAXS patterns of Nafion in terms of the spherical nature of the clusters. They suggested "an increase and a decrease in coherence of the intercluster spacings perpendicular and parallel to the extrusion direction, respectively". The possibility of deformation of the spherical clusters they rejected on the basis of their results. In this work and in the work of Rubatat et al.,[16,17] orientation in Nafion is discussed in terms of elongated polymeric aggregates.[8]

To quantify the orientation in a material, Hermans' orientation factor (or second-order Legendre polynomial) can be calculated:[18]

$$f = \frac{3\cos^2\varphi - 1}{2} \tag{1}$$

with φ the angle between the molecular chain axis and the deformation axis. A perfect orientation gives a value for f of 1, isotropic systems gives a value of 0, and perfect perpendicular alignment gives a value of −0.5. Different experimental techniques have been used to determine the orientation factor of polymeric systems, like for example birefringence, X-ray, infrared dichroism, laser-Raman spectroscopy, broad line nuclear magnetic resonance, and polarized fluorescence.[18,19] A combination of X-ray and birefringence experiments is frequently used to study the orientations of amorphous and (semi)-crystalline polymers, for example refs 20−25, and liquid crystalline polymers, e.g., refs 26−28. Orientation in ionomers is mainly studied by IR techniques.[29] Orientation in styrene-based ionomers is studied by Zhao et al.,[30] and it appeared that the presence of ionic clusters increases the orientation because they act as physical cross-links. Ding et al.[31] studied elastomer sulfonated polyurethanes and observed that orientation of chains in the polymer matrix was higher than in the ionic aggregates. More recent work of Wang et al.[32] on zwitterionomers with IR showed only a small orientation in the ionic region upon drawing. These examples show that the influence of an ionic group on the

* Corresponding author: e-mail odiat@cea.fr.

10.1021/ma035642w CCC: $27.50
Published on Web 06/17/2004

orientation within a polymer structure is not uniquely defined.

In this paper the orientation in Nafion on different length scales is studied with the help of Hermans' orientation factor. Elliot et al.[13] calculated the orientation factor for the Nafion 115 ionomer peak, and in the undrawn state a value of 0.2 was obtained, increasing up to 0.62 for a draw ratio of 150%. Upon applying the calculation of the orientation factor to other length scales than those determined from the ionomer peak position, we expect to get a complete picture of the structure of Nafion. We want to know the influence and type of orientation (rotation or chain distortion) at different length scales. Furthermore, we discuss the coherence between these orientation results and our "elongated polymeric aggregates" model for the structure of Nafion.

Experimental Section

Sample Preparation. Nafion 117 films (Aldrich, characterized by its equivalent weight (EW) = 1100 g equiv^{-1}) and Nafion 125 (EW = 1200 g equiv^{-1}) were used. The standard procedures are applied for the membrane preparation in terms of cleaning; the membrane is soaked twice for 2 h in HNO_3 (1 M). Then, it is immersed for 1 h in deionized water. In general, the acid form is used for our experiments. For the birefringence experiments, lithium (Li^+) and tetramethylammonium (TMA^+) neutralized forms are used. These neutralized forms are prepared by equilibrating the films in a saturated chloride solution for 2 days and renewing of the solution at least three times a day. Then the membrane is rinsed in pure water to remove the excess of salt.

SAXS and WAXS Experiments. Taking care of the processing direction of the film (the preorientation), a piece of the Nafion membrane (5 × 20 mm^2) is cut and placed in a homemade drawing cell. Using two coupled endless screws, a single membrane is stretched between two clamps, keeping the symmetry center of the deformation at the beam position. SAXS and WAXS 2D patterns are simultaneously recorded on the ID2 beamline at the ESRF.[33] The wavelength of the X-ray beam was 1 Å. Stacking membranes would improve the efficiency of the detection; however, it adds the problem of controlling the stretching without sliding of the different layers. The SAXS detector located at 1.5 m from the sample position (or 8 m for lower scattering angle detection) is an image intensified FReLoN CCD system, and the WAXS detector to measure the scattering over a larger q range is also an image intensifier CCD camera using an optical fiber system coupled to a 16 bit Princeton camera. We define the wave vector as $q = 4\pi/\lambda \sin(\theta/2)$, where θ is the scattering angle. Because of the off-centered position of the WAXS detector (it is located at 45° from the horizontal axis, see Figure 1A) which does not allow to record WAXS images over 360°, we have mounted the sample on a cradle. With this cradle, we are able to record scattering profiles simultaneously in SAXS and WAXS along the meridional and equatorial direction (parallel and perpendicular to the drawing direction, respectively) by rotating the sample around the beam path from −45° to +45°. This procedure is essential to obtain orthogonal scattering information since the WAXS detector is only covering a reduced scattering cone at large angles. The data acquisition time in each position is about 0.5 s, and the dead time between both positions is about 2 s. For example, 2D data in Figure 1B correspond to WAXS and to SAXS images obtained when the equatorial axis of the sample is oriented toward the WAXS detector. The dark region on the upper-right corner of the SAXS image corresponds to the shadow of the WAXS camera support, reducing the SAXS detection field. Data treatment follows standard procedures for transmission, flat field, and distortion corrections. The transmission is determined using a photodiode located into the beamstop. The setup allows a slight overlap in scattering angle between both detections.

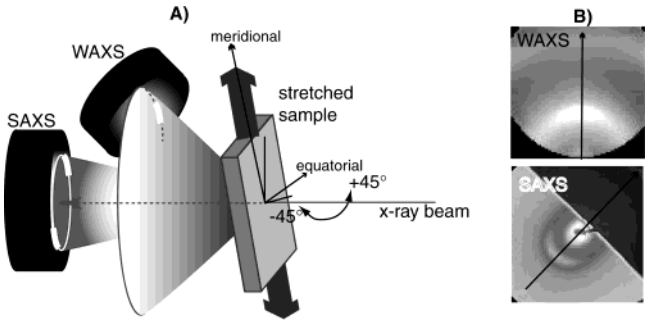

Figure 1. Schematic setup combined WAXS and SAXS experiment. (A) The SAXS camera is as usual located along the beam axis, and the WAXS detector is off-centered (located at 45° of the beam axis). As an example, WAXS and SAXS 2D images are displayed in (B), corresponding to a sample position on the cradle with the stretching direction at −45°. The equatorial axis is indicated on both scattering images. When the SAXS detector is at less that 2 m from the sample position, a shadow of the WAXS detector support is observable on the SAXS image at the upper right corner.

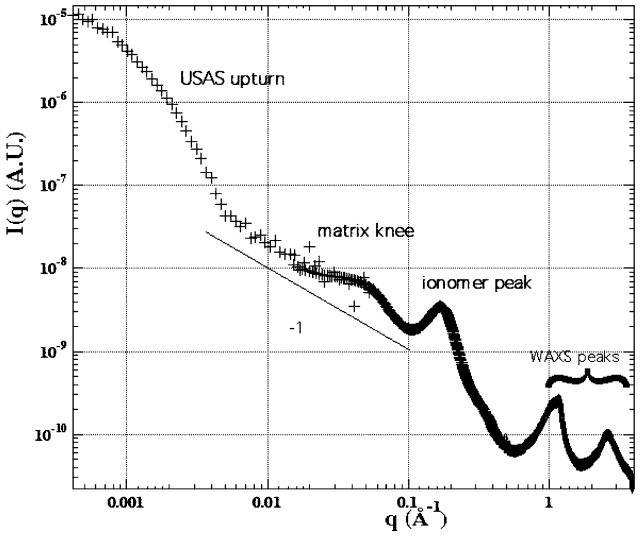

Figure 2. Combined WAXS, SAXS, and USAXS results of water swollen Nafion 117 neutralized with lithium.

Results and Discussion

Figure 2 shows a combined X-ray scattering result for a large wave vector range (q) of swollen Nafion 117. Using the terminology of refs 1 and 8, we can distinguish for the SAXS experiments (from small to large q values): the USAXS upturn which is attributed to large-scale electron density inhomogeneities in the range of thousands of angstroms and corresponding to an orientation correlation scale for the polymeric aggregates, the matrix knee which is characterized as the correlation distance between the crystalline parts along the polymeric aggregates, and the ionomer peak which is analyzed as the distance between polymeric aggregates ($q = 0.15$ Å^{-1}).[9] The WAXS results show an amorphous peak with a superimposed crystalline peak at q = 1.1 Å^{-1} and $q = 1.24$ Å^{-1}, respectively.[34] Finally, at a q value of $q = 2.75$ Å^{-1} a peak not frequently described is observed. The Bragg distance (2.28 Å) might be interpreted as an intrachain distance of a Nafion chain.

The ionomer peak, amorphous peak, crystalline peak, and peak 3 are subjected to our orientation analysis. In the following section the data treatment procedures are described to obtain plots of the maximum intensity against the azimuthal angle for the four peaks.

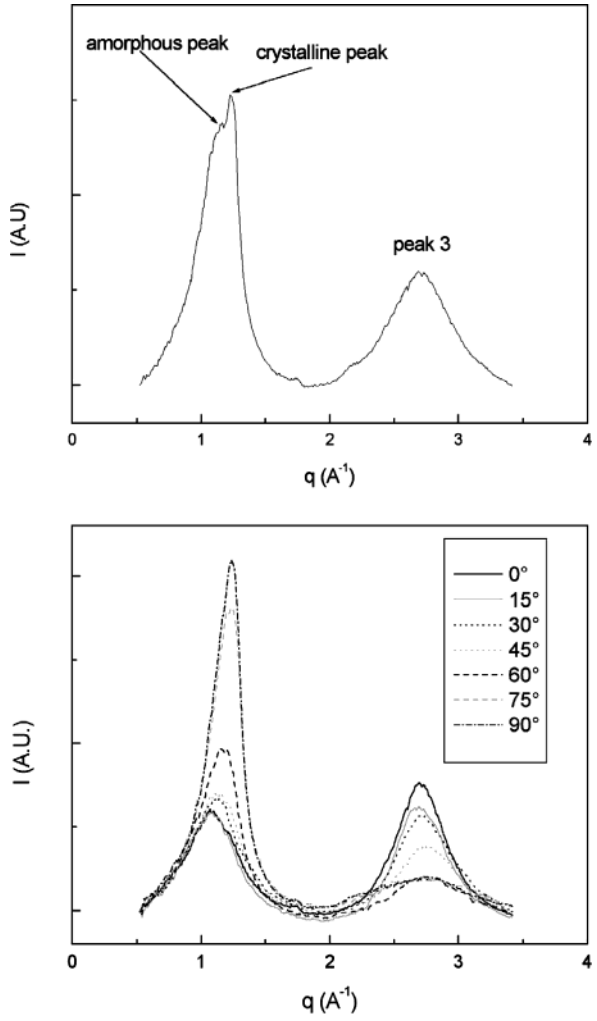

Figure 3. WAXS results of Nafion 125: at meridian for DR = 100% (top picture) and for DR = 229% for different azimuthal angles (bottom picture).

WAXS: Data Treatment. Figure 3 shows results of Nafion 125, with the definitions of the different peaks (top picture) and for different azimuthal angles (bottom picture). The draw ratio (DR) is defined as the ratio of the distance between two marks on the drawn film, and this distance in the undrawn state. The peaks already identified can be distinguished from these figures: the amorphous peak at $q = 1.1$ Å^{-1}, a small and weak peak superimposed on the amorphous peak (at $q = 1.24$ Å^{-1}) which is the crystalline peak,[5] and a peak at $q = 2.75$ Å^{-1} (peak 3). In the Appendix the peaks are interpreted by comparing different models for the crystalline phase of Nafion. It appeared that the crystalline peak is caused by intermolecular distances and that the broad peak 3 consists of several diffraction peaks from intramolecular correlations.

To obtain figures of the maximum intensity as a function of the azimuthal angle for the WAXS peaks, the following procedure is applied. For each draw ratio, intensity−q plots are extracted from the 2D WAXS pattern for azimuthal angles of 0° (meridian), 15°, 30°, 45°, 60°, 75°, and 90° (equator). After subtraction of a linear baseline, the WAXS spectra are fitted with three Lorentzian functions to obtain values for the peak positions and heights corresponding to the amorphous and the superimposed crystalline peaks (see Figure 4).

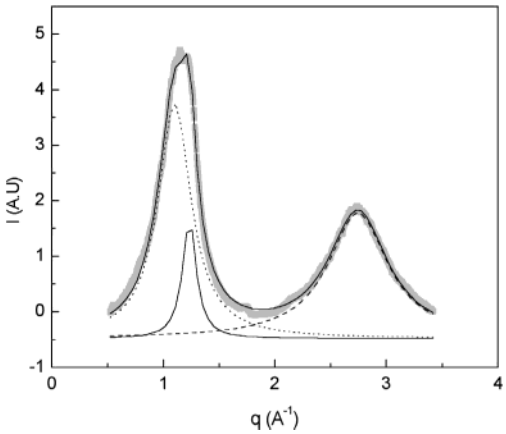

Figure 4. Fit for Nafion 117, DR = 100% for the meridional direction. The gray dots represent the experimental (baseline corrected) curve. The dotted line represents the amorphous peak, the solid line the crystalline peak, and the dashed line represents peak 3.

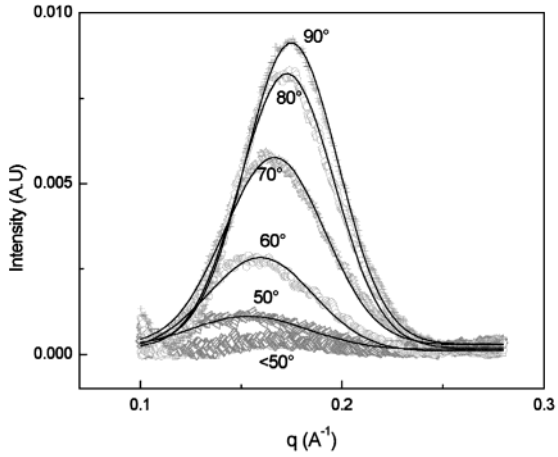

Figure 5. Ionomer peak as a function of q for different azimuthal angles for Nafion 117, DR = 143%. Gray dots represent the experimental data and black lines the Gaussian fits.

We consider that peak 3 can be assimilated to a single diffraction peak in a first approach.

SAXS: Data Treatment. To obtain the maximum intensity of the ionomer peak from the SAXS results, a linear baseline is subtracted from the data, and a Gaussian function is used to obtain peak height and position (example in Figure 5).

For azimuthal angles below 50° and draw ratios over 108%, it was difficult to obtain reliable Gauss fits because of the very small peaks in comparison with the scattering of data. The observed shift to lower q values, and the disappearance of the ionomer peak in the meridional position for higher draw ratios is in agreement with other work.[14]

Radial and Azimuthal Distribution. The ionomer, amorphous, crystalline, and peak 3 positions are plotted in Figure 6 as a function of the draw ratio for the meridian (0°, solid line) and the equator (90°, dotted line). It can be observed that the peak positions in the meridional and equatorial direction of the crystalline peak do not change upon drawing. On the contrary, the ionomer, the amorphous, and peak 3 positions show a decrease in q value in the meridional direction with increasing draw ratio.

Figure 7 shows the maximum intensities as a function of the azimuthal angle for the different draw ratios. For

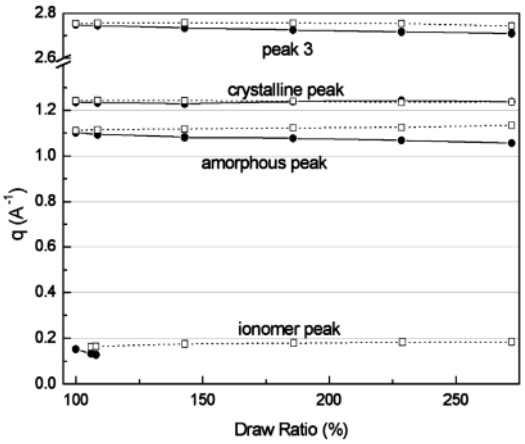

Figure 6. Crystalline, amorphous, and ionomer peaks positions of Nafion 117 as a function of the draw ratio. Solid line: azimuthal angle is 0° (meridian). Dotted line: azimuthal angle is 90° (equator).

a fair comparison between different draw ratios, the intensities are divided by the thickness of the film according to a relation based on experiments in our previous paper.[10] This is necessary because upon drawing the thickness decreases, and hence less scattering entities are present. This correction has no influence on the calculation of the orientation factor and crystallinity treated later in this work. The ionomer peak, amorphous peak, and crystalline peak show an increasing intensity with increasing azimuthal angle, and peak 3 shows the inverse trend. These observations are discussed in more detail later in this work. Before using Figure 7 to calculate Hermans' orientation factor, we first discuss the crystallinity and the interpretation of peak 3.

Crystallinity. To a first approximation the crystallinity (x_c) can be calculated by integrating the crystalline intensity and the total intensity over all reciprocal space.[35] For an isotropic system this can be written as

$$x_c = \frac{\int_0^\infty q^2 I_c(q)\, dq}{\int_0^\infty q^2 I(q)\, dq} \qquad (2)$$

In our case we deal with an anisotropic system, and (2) has to be rewritten to take into account an intensity which depends on the azimuthal angle. Using the 2D

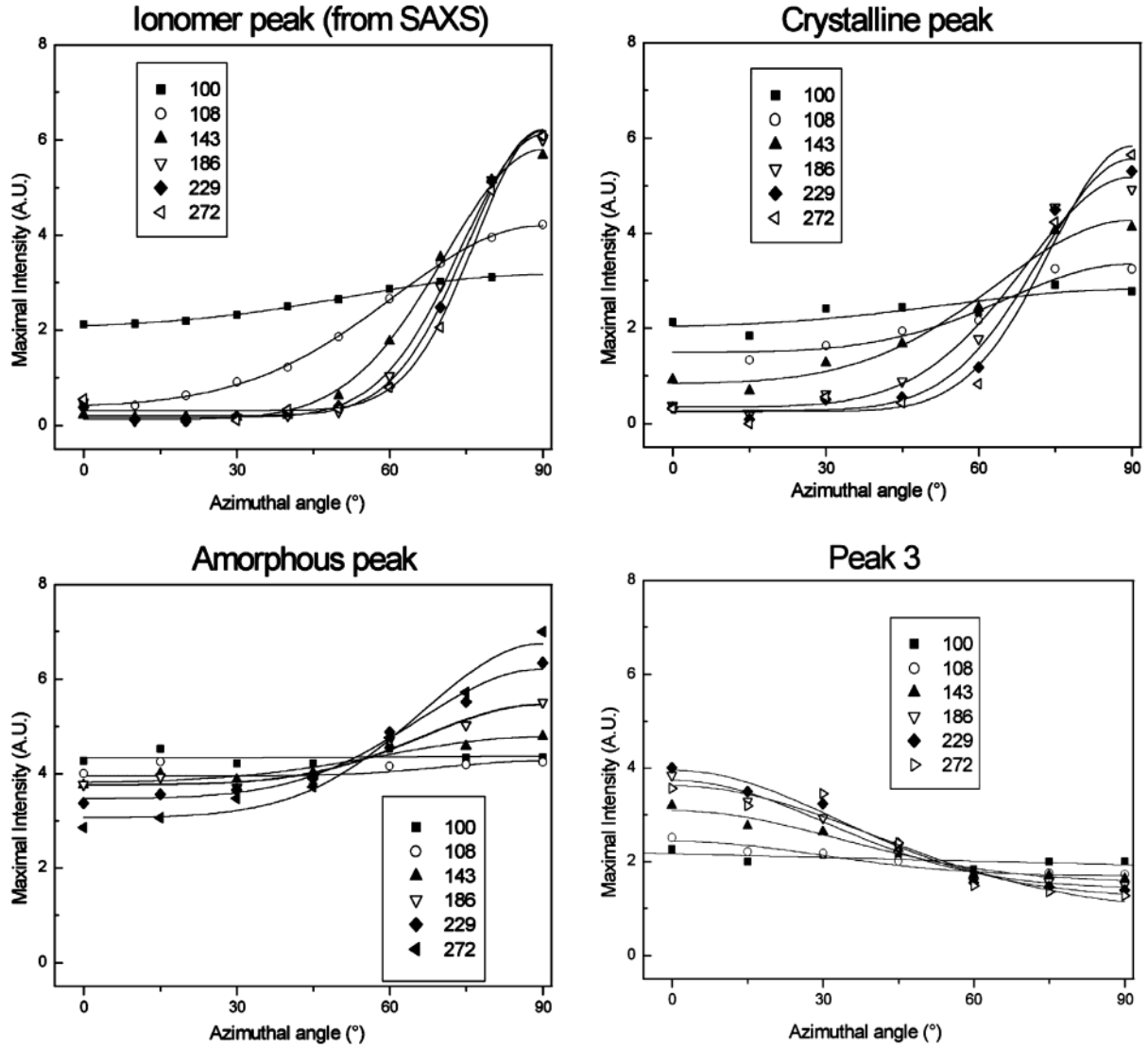

Figure 7. Maximum intensities vs azimuthal angle (0° is meridian and 90° is equator) of Nafion 117 for different draw ratios for the different peaks.

Table 1. Crystallinity (x_c) as a Function of the Draw Ratio

DR (%)	Nafion 117	Nafion 125	DR (%)	Nafion 117	Nafion 125
100	0.22	0.20	229	0.17	0.19
143	0.21	0.23	272	0.18	0.22
186	0.19	0.19			

Table 2. Ratio Amorphous and Crystalline Peak to Peak 3 (x_3)

DR (%)	Nafion 117	Nafion 125	DR (%)	Nafion 117	Nafion 125
100	0.35	0.36	229	0.35	0.38
143	0.34	0.35	272	0.36	0.39
186	0.34	0.36			

X-ray data, we summed over the azimuthal angle, multiplied this by q^2 and integrated over q:

$$x_c = \frac{\int_0^\infty \int_0^{\pi/2} I_c(q,\varphi) q^2 \, d\varphi \, dq}{\int_0^\infty \int_0^{\pi/2} I(q,\varphi) q^2 \, d\varphi \, dq} \tag{3}$$

with φ the azimuthal angle and $I = I_a + I_c$, with I_a and I_c the intensities of the amorphous and crystalline peak, respectively.

Instead of integrating over q values between 0 and infinite, we integrated between 0 and $q_{max} = 3.4$ Å^{-1}, which corresponds to the highest q value of the fit of our WAXS results. Table 1 lists the values of x_c for both Nafion types.

The average crystallinity over all the draw ratios is 0.193 ± 0.017 for Nafion 117 and 0.204 ± 0.014 for Nafion 125. For undrawn Nafion, Fujimura[34] calculated the crystallinity assuming complete isotropy (according to eq 2) and found a value of 0.12 for Nafion 117 H^+ and 0.19 for Nafion 125. From an IR study,[36] a crystallinity of 0.25 was observed for Nafion 117. The most important conclusion of this calculation of the crystallinity is that no significant change in crystallinity is observed as a function of the draw ratio. The frequently observed phenomena of a stress-induced crystallization in polymers (e.g., refs 37 and 38) is not observed for Nafion, probably because of the influence of the ionic groups in Nafion which prohibits the presence of large crystalline domains. Moreover, whereas the crystalline peak is more pronounced for Nafion 125 than for Nafion 117, the degree of crystallinity does not strongly differ and suggests that mainly the size and not the amount of the crystalline region is changing by varying the equivalent weight.

Interpretation of Peak 3. To verify our hypothesis that peak 3 is caused by overlapping diffractions from intrachain correlations, we define the ratio of diffracting planes of the amorphous and crystalline peak with peak 3 as

$$x_3 = \frac{\int_0^\infty \int_0^{\pi/2} I(q,\varphi) q^2 \, d\varphi \, dq}{\int_0^\infty \int_0^{\pi/2} I_3(q,\varphi) q^2 \, d\varphi \, dq} \tag{4}$$

Table 2 lists the values for peak 3 (x_3):

x_3 is interpreted as the ratio between the amount of diffracting planes parallel and perpendicular to the polymer chain. The density of the diffracting planes in a given direction can be expressed as

$$n = d^{-1} \tag{5}$$

with d the distance between the planes.

When assuming a Nafion monomer which only diffracts along the chain axis and perpendicular to it, the theoretical value of x_3 should have a value of

$$x_3 = \frac{n_{perp}}{n_{par}} = \frac{d_3}{d_a} = \frac{q_a}{q_3} \tag{6}$$

with q_a and q_3 the q values of the peak maximum of the amorphous peak and peak 3.

In our case $x_3 = 1.1/2.75 = 0.4$. This number agrees well with the values in Table 2, which indicates that peak 3 is the result from diffraction of both the amorphous and crystalline phases along the chain axis of Nafion.

Orientation. Originally, the theory to calculate the orientation factor was derived for well-defined crystal phases. The orientation factor of a crystal plane with the normal in the a direction, and the drawing direction in the Z direction ($f_{a,Z}$) can be calculated according to (7).[35]

$$f_{a,Z} = {}^1/_2(3\langle \cos^2 \varphi_{a,Z} \rangle - 1) \tag{7}$$

$$\langle \cos^2 \varphi_{a,Z} \rangle = \frac{\int_0^{\pi/2} I(\varphi) \sin \varphi \cos^2 \varphi \, d\varphi}{\int_0^{\pi/2} I(\varphi) \sin \varphi \, d\varphi} \tag{8}$$

$$f_{a,Z} + f_{b,Z} + f_{c,Z} = 0 \tag{9}$$

with a, b, c the crystal directions and φ the angle between a given crystal direction and the draw direction, Z. In eq 8, $I(\varphi)$ is the intensity of the diffraction in direction a. For orthogonal crystals, the sum of the orientation factors in the three directions is 0 (eq 9).

In the equatorial direction, the crystalline peak (representing the interchain distance) is increasing in intensity with increasing draw ratio (as observed in Figure 7). This indicates that more chains are aligned along the meridional direction upon drawing. From this, we conclude that the Nafion chains in the crystalline phase orient parallel to the draw direction. The amorphous peak and the ionomer peak show the same trend. Negative values for the orientation factors are determined from their azimuthal distribution. Peak 3 is decreasing with an increasing draw ratio, less scattering entities are in the diffraction plane, and a positive value for f upon drawing is obtained. Assuming an orthorhombic structure for the crystalline part of Nafion, as proposed in the Appendix, perfect alignment is achieved when the c axis (which is along the chain direction) is parallel to the draw direction. The diffractions in the a and b directions are thus perpendicular to the draw direction.

To quantify these considerations, a Gaussian function is drawn through the results of the intensity vs the azimuthal angle. The orientation factors for the four peaks are plotted in Figure 8 as a function of the draw ratio. The error bars are determined from the errors in the coefficients from the Gaussian fit. The curve of the ionomer peak of Nafion 125 is not as nice as those for Nafion 117, and the error bars are larger. This is caused by the fact that the equivalent weight of Nafion 125 is higher; therefore, the ionomer peak is less pronounced as for Nafion 117, and it is more difficult to extract accurate data for this peak. From Figure 8, it can be observed that the ionomer peak reaches the maximum orientation at lower draw ratios than the crystalline

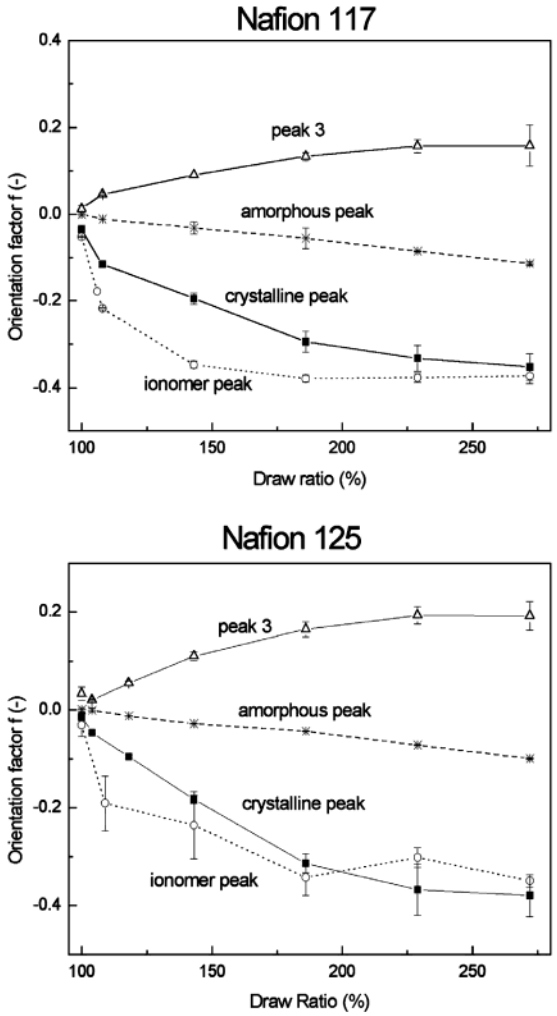

Figure 8. Orientation factors of the different peaks of Nafion 117 (top) and Nafion 125 (bottom) as a function of the draw ratio.

peak, at least for Nafion 117. This effect is present, but less pronounced, for Nafion 125 as well. This means that the orientation is different at the scale of several ionomer distances in comparison with the scale of several chains distances, in agreement with the observations in ref 13. This mechanism of orientation can be described in two steps as explained in the section "Interpretation of Orientation Results".

To compare the origin of the orientation of the different peaks, we have to keep in mind that the observed azimuthal profiles are the results of the convolution between the true orientation distribution function and the intrinsic profile. The distances between or in a molecule in the amorphous phase have a broader distribution than in the crystalline phase, which give a broader azimuthal profile in the amorphous phase for the same orientation factor. To correct for this intrinsic azimuthal width, the azimuthal half-width can be determined according to

$$\delta = \frac{\int_0^{\pi/2}[I(\varphi) - I(0)]\,\mathrm{d}\varphi}{I(\pi/2) - I(0)} \qquad (10)$$

and this value can be plotted as a function of the inverse of the draw ratio[22] or the observed orientation factor[24] in order to determine the intrinsic azimuthal width (by extrapolation to $DR^{-1} = 0$ and $f = 1$, respectively).

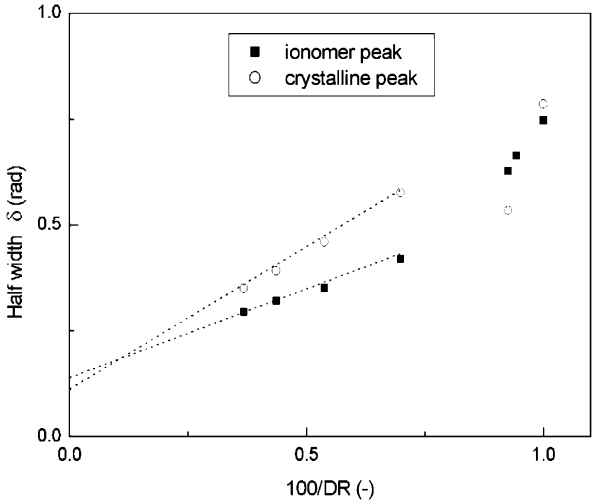

Figure 9. Azimuthal width of the ionomer peak and the crystalline peak of Nafion 117 as a function of the inverse draw ratio to determine the intrinsic azimuthal width. The extrapolation to a perfect oriented system ($DR^{-1} = 0$) is given by the dotted lines.

Table 3. Intrinsic Azimuthal Width and Correction Factor According to Ref 22 of Nafion 117

peak	correction factor
ionomer	1.1
amorphous	1.5
crystalline	1.1
peak 3	2.0

Figure 9 shows the results for the ionomer peak and the crystalline peak as a function the reciprocal draw ratio. For the two other peaks (the amorphous peak and peak 3) the intrinsic widths are larger. In the case of amorphous systems, an infinite draw ratio cannot lead to a perfect orientation, and a procedure was developed to correct the Hermans' orientation factor taking into account the intrinsic width extrapolation.[22,24,26] These correction factors can be determined with the help of Figure 5 of ref 22 and are listed in Table 3 for the four peaks. From this table, it can be observed that the correction factor for both crystalline and the ionomer peaks are identical. Therefore, we have the interesting possibility to compare the orientation factors of the ionomer peak and the crystalline peak in a direct way, without using correction factors. We can remark that this value is 1.1, a value which is close to the theoretical value of crystalline system (=1).

This comparison allows to correlate the drawing effect on the polymeric film at two different length scales: the mesoscopic scale which is characterized by the ionomer peak and the molecular scale which is characterized by the crystalline peak. We can define the ratio α between both orientation factors and as a function of the draw ratio to analyze the evolution of this correlation. This concept is used in polymer liquid crystals[27,39,40] and allows taking into account separately the mesoscopic and the molecular orientation. A ratio of 1 between these factors means that the degree of orientation is similar on both scales.

This ratio α between the crystalline and ionomer orientation factors is plotted in Figure 10 for both Nafion 117 and Nafion 125. At the first sight, α is different than 1 and increases as a function of the draw ratio from 0.5 up to 1. An almost perfect orientation of the polymer chains in the crystal phase within the

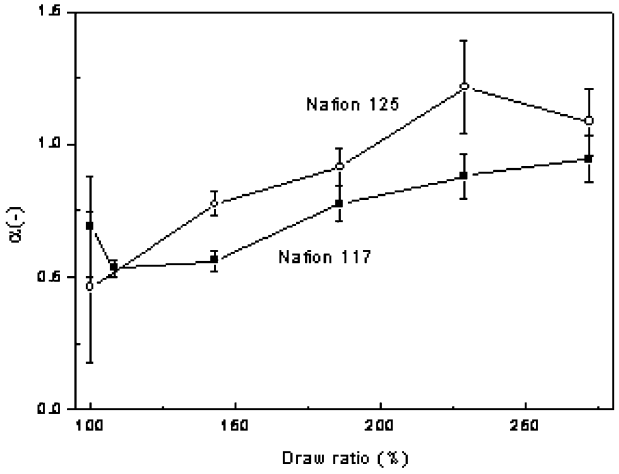

Figure 10. α, the ratio between the crystalline and ionomer orientation factors, as a function of the draw ratio.

mesoscopic scale ($\alpha \approx 1$ and f close to -0.5) is achieved at large draw ratios. The interpretation of this orientation correlation between the mesoscopic and molecular scales is discussed in more detail in next section. Furthermore, it is striking to observe that, after reaching this maximum orientation, the polymer film breaks.

Interpretation of Orientation Results. In this section, the observed results are discussed in the frame of existing models of swollen Nafion. We have shown in a previous publication that the Gierke model cannot be applied for the Nafion structure;[7] however, we can consider the case of water swollen spherical ionic clusters (with a distance between two pools being of the same order as the pool size) dispersed in a polymeric matrix. The stretching effect on this type of structure is described in terms of the deformation of the water pools (characterized by the ionomer peak in the scattering geometry). They have a spherical shape in the undrawn state and an ellipsoidal shape under deformation. The deformation of the water pools should have a strong dependency on the orientation of the polymer chains at the interface and in the polymer matrix, characterized by the crystalline and amorphous peaks. Thus, the orientation of both the ionomer and crystalline peaks should vary with the same trend; in other words, α has to be equal to 1. The fact that the orientation factor of the ionomer peak is a different function of the draw ratio than the crystalline peak (see Figure 8 or 10, $\alpha < 1$) is sufficient to reject the possibility of the deformation of the hydrophilic pools (that cannot be deformed more than the surrounding polymeric material).

Starkweather[41] proposed a bilayered crystal phase between the water pools. Upon stretching, it is possible that the water pools surrounded by the bilayered crystal phase do not deform; however, the water pools surrounded by the amorphous phase have to deform (otherwise, no change in ionomer peak can be observed). Assuming this mechanism, we have to observe an increase in the azimuthal half-width of the ionomer peak as a function of the draw ratio because the orientation distribution of the ionomer increases. This trend is in contrary to our results in Figure 9, in which the azimuthal width decreases. Also, this physical picture can be rejected on the basis of our results.

Taking into account a fibrillar structure as developed in refs 8 and 9 in which we consider the Nafion structure as a collection of elongated polymeric aggregates in bundles, we can describe our experimental observations. Indeed, the fact that the orientation factor differs between the mesoscopic scale and the molecular scale means that there exists a cutoff in size which characterizes two different structural orientation effects. If we consider the elongated polymeric aggregates consisting of more or less ordered chains as the basic entities in the Nafion structure, this cutoff corresponds to the diameter of these aggregates. Starting with this picture, we can describe the orientation process in Nafion films as follows. Upon stretching, two mechanisms are simultaneously present: the first one corresponds to the rotation of large bundles (in which the elongated aggregates are more or less correlated in orientation) and which is described by the orientation factor of the ionomer peak. The second mechanism corresponds to a better alignment of the aggregates within the bundles; due to sliding or disentangling of the aggregates from each other, this is described by the orientation factor of the crystalline peak. The first mechanism is predominant at small draw ratios, while the second mechanism mainly takes place at higher draw ratios. In Figure 11, a rough sketch is presented to give an insight on both orientation mechanisms. The orientation in the amorphous phase is, even when the correction factor from Table 3 is applied, much smaller upon drawing than for the crystalline phase. Probably, chain distortion of the amorphous phase takes place upon stretching whereas with the crystalline peak only orientation takes place (see Figure 6 in which the peak position of the crystalline peak is constant, and the peak position of the amorphous peak shifts as a function of the draw ratio).

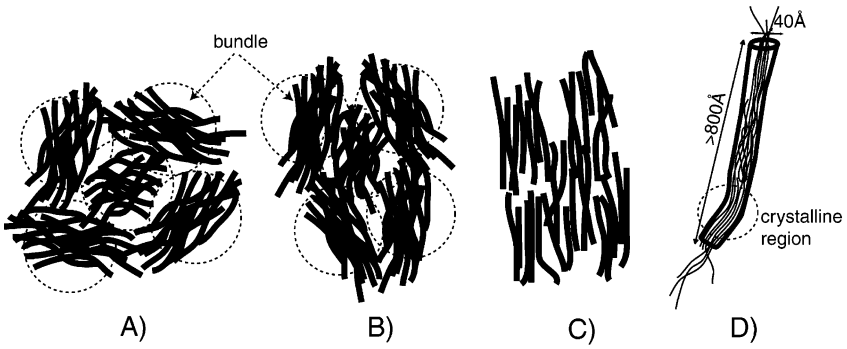

Figure 11. Sketch of fibrillar structure of Nafion:[16] (A) organization of bundles of elongated aggregates made of more or less aligned and ordered polymeric chains surrounded with ionic groups and water molecules (a magnification of an aggregate is depicted in image D, the surrounding ionic groups are not drawn). Under stretching (vertical direction), the large domains or bundles are rotating (B), and then at higher strain the aggregates are oriented within a bundle (C).

A different approach to study the Nafion structure is carried out using birefringence techniques and with mechanical experiments analysis in which the creep of drawn Nafion is studied. It appears that both mechanisms of orientation can be observed as well and will be described as a function of water content and the nature of counterion in a future publication.[42]

If we assume that a higher equivalent weight gives larger ordered parts inside the aggregates, then we can suppose that the aggregates are more rigid. These aggregates will be better aligned inside the bundles. Consequently, for Nafion 125, the orientation effect of the crystallites inside the aggregates is more correlated with the orientation of the aggregates in the bundles than for Nafion 117 (which is observed in Figure 8). To confirm this tendency, a study should be performed on a larger variation of equivalent weights in order to analyze the effect of crystallinity.

Conclusion

Using SAXS and WAXS techniques, we have recorded the 2D X-ray scattering intensity of Nafion films as a function of the draw ratio. We determined the azimuthal distribution function at different q-vector positions, corresponding to the ionomer, amorphous, and crystalline peaks. We quantified this distribution using the Hermans' orientation factor for each of them in order to analyze their correlations as a function of the drawing ratio. We showed that the orientation effects at the "ionomer" and molecular scales are not equal; this difference disappears at a large draw ratio and can be perfectly analyzed in the frame of a fibrillar model of the Nafion structure, made of elongated polymeric aggregates. Two mechanisms are revealed upon stretching that can be interpreted as (1) the rotation of bundles of aggregates at small draw ratios and (2) the orientation increase of the aggregates within a bundle, the second becoming predominant at large draw ratio.

In the future we will show that the coupled analysis between the birefringence and the X-ray scattering data allows us to obtain the values for the intrinsic amorphous and crystalline, which are reasonable in comparison with published data for aliphatic polymers. Moreover, we will use this optical property and these values to determine the internal stress of the film under strain.

Acknowledgment. A. De La Rosa and G. Gebel are acknowledged for discussions. The ID2 beamline team is acknowledged for its experimental help as well as the ESRF for generously allocating the beamtime (allocation SC1150). We thank W. G. Grot for kindly supplying the Nafion 125 films.

Appendix. Crystal Structure of Nafion

It is commonly agreed that Nafion is a semicrystalline ionomer because of the presence of the polytetrafluorethylene (PTFE) backbone.[3] However, the type of unit cell and corresponding distances is still a debate. Starkweather[41] proposed a hexagonal unit cell with length of $a = 5.8$ Å and $c = 2.6$ Å (direction along the chain axis). His work was based on oriented and unoriented Nafion fibers. Ludvigsson[43] casted Nafion films and irradiated the film with Xenon ions to introduce crystalline regions. They observed an orthorhombic unit cell like polyethylene (PE) with a linear zigzag structure of the polymer backbone. Porat[44] observed a comparable structure with electron microscopy experiments. They deposited Nafion from solution directly on a carbon-coated TEM grid, or they formed a Nafion film on mica before placing on the TEM grid. The unit cell dimensions obtained from the experiments were different in both studies. Ludvigsson proposed unit cell dimensions of $a = 6.64$ Å and $b = 5.44$ Å; Porat found $a = 7.49$ Å and $b = 5.02$ Å. They were not able to determine the distance in the c-direction. Upon following the analogy with polyethylene, it is possible to estimate the unit cell size in the c-direction, for PE $c = 2.54$ Å (for completeness: $a = 7.40$ Å and $b = 4.94$ Å).[45] With these dimensions of the unit cell and the fact that one unit cell consists of two PTFE monomers, it is possible to calculate the density of the crystalline phase.[45] This gives values of 3.3 g cm^{-3} (Porat) and 3.5 g cm^{-3} (Ludvigsson). Literature values for PTFE (2.3 g cm^{-3})[45] and Nafion (2.1 g cm^{-3}, amorphous and crystalline parts together)[4,5] show much lower values. Even when the distance c is raised to 3 Å, unrealistic high densities are obtained. Hence, the unit cells sizes proposed by Porat and Ludvigsson are not applicable for standard Nafion films. Nafion consists of a PTFE backbone; therefore, a comparison with the crystal data of PTFE polymers is made as well. The polymer handbook gives for PTFE for $T > 20$ °C a twisted hexagonal structure. Different twist values and lattice parameters (only small differences) are proposed; we choose for a lattice consisting of 15 CF_2 groups with a lattice size of $a = b = 5.66$ Å and $c = 19.5$ Å. Calculating the density based on the lattice dimensions gives a value of 2.3 g cm^{-3}.

Table 4. Lattice Planes and q Spacing for Nafion SO_2F and H^+

Nafion SO_2F		Nafion 117 H^+		fit orthorombic	
q (Å^{-1})	intensity	q (Å^{-1})	intensity	plane	q (Å^{-1})
1.27	high	1.24	high	⟨200⟩	1.27
1.73	low	1.70	low	⟨210⟩	1.69
1.95	medium			⟨300⟩	1.90
2.26	high			⟨001⟩/⟨020⟩	2.24
2.78	broad	2.75	broad	⟨211⟩	2.81[a]
3.18	medium			⟨021⟩	3.17[a]

[a] Many other (higher value Miller indices) planes give a solution close to these values. This is maybe also an explanation for the broad peak around $q = 2.8$ Å^{-1}.

X-ray experiments on the precursor of Nafion, the SO_2F form, show sharp diffraction peaks as listed in Table 4. The peaks found for Nafion H^+ films in this work are listed as well. To contribute to the discussion about the structure of the crystal phase of Nafion, our experimental results were fitted with an orthorhombic cell:[35]

$$d = \left[\left(\frac{h}{a}\right)^2 + \left(\frac{k}{b}\right)^2 + \left(\frac{l}{c}\right)^2\right]^{-1/2} \tag{11}$$

with d the interplanar spacing, a, b, c the unit-cell dimensions, and h, k, l the Miller indices of the refraction planes.

The obtained unit cell dimensions are $a = 9.9$, $b = 5.6$, and $c = 2.8$ Å. The q values for planes belonging to this unit cell are listed in the last two columns of Table 4. The calculated crystal density of this unit cell is 2.05 g cm^{-3}.

To compare the different models to our experimental data, the diffraction peaks are calculated for the model of Starkweather, PTFE, and our orthorhombic model

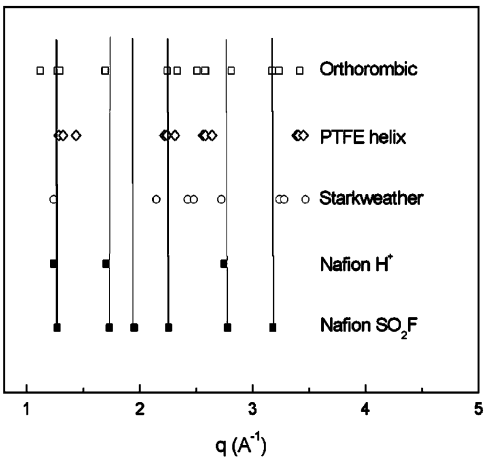

Figure 12. Comparison proposition Starkweather,[41] PTFE helix,[45] and our fit with a orthorhombic model for Miller indices to 2. The black lines represent large peaks, and the gray lines represent smaller peaks.

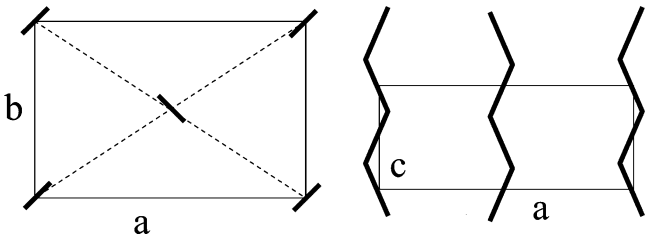

Figure 13. Schematic unit cell; only the monomers of the carbon backbone of PTFE are drawn (drawn on the base of the structure of polyethylene[46]).

(only Miller indices equal or smaller than 2 were used) and plotted in Figure 12. The comparison between the different models is made with the experimental results of Nafion SO_2F. This precursor shows higher crystallinity and is not influenced by ionic interactions as is the case for Nafion H^+. Starkweather[41] mentioned that the crystal sizes in the acid form were smaller or less perfect than in the F form. In this work we assume that the crystal type is equal for the precursor and acidic form of Nafion.

None of the models can describe the experimental diffraction pattern exactly up to Miller indices of 2. Because of the large *c*-direction in the PTFE helix model, many peaks of the form $\langle 10x \rangle$ or $\langle 01x \rangle$ has to be found from q values of 1.6 $Å^{-1}$ and higher. However, these peaks are not observed in our experimental results. The model of Starkweather gives no extra diffraction between $q = 1.5$ and 2 $Å^{-1}$ for higher Miller indices; hence, this model describes our experimental results not very accurate as well. Our orthorhombic model misses a peak at $q = 1.95$ $Å^{-1}$. When taking into account higher Miller indices, it appears that the missing peak can be described by the $\langle 300 \rangle$ plane. This is a strong indication that our orthorhombic model is the best choice.

From these considerations we conclude that the crystalline phase in Nafion consist of PTFE chains in an orthorhombic unit cell with dimensions $a = 9.9$ Å, $b = 5.6$ Å, and $c = 2.8$ Å. The value of c is in good agreement with the van der Waals radius of the fluorine atom, 1.4 Å;[35] maybe the structure is slightly twisted as proposed by ref 36. They proposed a unit cell with a c value of 1.7 nm and 6 monomers; this gives a distance of 2.8 Å between the monomers. However, they did not distinguish between the amorphous and crystalline phase. A schematic picture of the (nontwisted) orthorhombic structure is drawn in analogy of the polyethylene structure[50] in Figure 13. To study the orientation of Nafion H^+, the most reliable information can be obtained from the peak at $q = 1.24$ $Å^{-1}$, the $\langle 200 \rangle$ plane. The other signals either have a plane with an angle different than either 0 or 90° with the draw direction (peak at $q = 1.70$ $Å^{-1}$) or are not uniquely defined (peak at $q = 2.75$ $Å^{-1}$).

References and Notes

(1) Schlick, S. *Ionomers, Characterization, Theory and Applications*; CRC Press: Boca Raton, FL, 1995.
(2) Heitner-Wirguin, C. *J. Membr. Sci.* **1996**, *120*, 1−33.
(3) Tant, M. R.; Mauritz, K. A.; Wilkes, G. L. *Ionomers. Synthesis, Structure, Properties and Applications*; Blackie Academic & Professional: London, 1997.
(4) Loppinet, B.; Gebel, G.; Williams, C. *J. Phys. Chem. B* **1997**, *101*, 1884−1892.
(5) Gierke, T. D.; Munn, G. E.; Wilson, F. C. *J. Polym. Sci., Polym. Phys.* **1981**, *19*, 1687−1704.
(6) Gebel, G. *Polymer* **2000**, *41*, 5829−5838.
(7) Rollet, A.-L.; Diat, O.; Gebel, G. *J. Phys. Chem. B* **2001**, *106*, 3033−3036.
(8) Rubatat, L.; Rollet, A.-L.; Gebel, G.; Diat, O. *Macromolecules* **2002**, *35*, 4050−4055.
(9) Rubatat, L.; Gebel, G.; Diat, O. Submitted to *Macromolecules*.
(10) Van der Heijden, P. C.; Bouzenad, F.; Diat, O. *J. Polym. Sci., Polym. Phys.*, in press.
(11) Fujimura, M.; Hashimoto, T.; Kawai, H. *Macromolecules* **1982**, *15*, 136−144.
(12) Cable, K. M.; Mauritz, K. A.; Moore, R. B. *Polym. Prepr.* **1994**, *35*, 421−422.
(13) Elliott, J. A.; Hanna, S.; Elliott, A. M. S.; Cooley, G. E. *Macromolecules* **2000**, *33*, 4161−4171.
(14) Londono, J. D.; Davidson, R. V.; Mazusr, S. *Polym. Mater. Sci. Eng.* **2001**, *85*, 23−24.
(15) Landis, F. A.; Moore, R. B.; Page, K. A.; Han, C. C. *Polym. Mater. Sci. Eng.* **2002**, *87*, 121−122.
(16) Rubatat, L.; De la Rosa, A.; Van der Heijden, P. C.; Gebel, G.; Diat, O. To be submitted.
(17) Rubatat, L. Thesis in Physics; Université Joseph Fourier: Grenoble, 2003.
(18) Ward, I. M. *Structure and Properties of Oriented Polymers*; Applied Science Publishers Ltd.: London, 1975.
(19) Ward, I. M. *J. Polym. Sci., Polym. Symp.* **1977**, *58*, 1−21.
(20) Hoshino, S.; Powders, J.; Legrand, D. G.; Kawai, H.; Stein, R. S. *J. Polym. Sci.* **1962**, *58*, 185−204.
(21) Samuels, R. J. *J. Polym. Sci., Part A* **1965**, *3*, 1741−1763.
(22) Pick, M.; Lovell, R.; Windle, A. H. *Polymer* **1980**, *21*, 1017−1024.
(23) Spector, K. S.; Stein, R. S. *Macromolecules* **1991**, *24*, 2083−2089.
(24) Vancso, G.; Snétivy, D.; Tomba, I. *J. Appl. Polym. Sci.* **1991**, *42*, 1351−1359.
(25) Voice, A. M.; Bower, D. I.; Ward, I. M. *Polymer* **1993**, *34*, 1154−1163.
(26) Van Aerle, N. A. M.; Tol, A. J. W. *Macromolecules* **1994**, *27*, 6520−6526.
(27) Beekmans, F.; Posthuma de Boer, A. *Macromolecules* **1996**, *19*, 8726−8733.
(28) Hongladarom, K.; Ugaz, V. M.; Cinader, D. K.; Burghardt, W. R.; Quintana, J. P.; Hsiao, B. S.; Dadmun, M. D.; Hamilton, W. A.; Butler, P. D. *Macromolecules* **1996**, *29*, 5346−5355.
(29) Grady, B. P.; Cooper, S. L. In *Ionomers. Synthesis, Structure, Properties and Applications*; Tant, M. R., Mauritz, K. A., Wilkes, G. L., Eds.; Blackie Academic & Professional: London, 1997.
(30) Zhao, Y.; Bazuin, G.; Prud'homme, R. E. *Macromolecules* **1989**, *22*, 3788−3793.
(31) Ding, Y. S.; Register, R. A.; Yang, C.-z.; Cooper, S. L. *Polymer* **1989**, *30*, 1204−1212.
(32) Wang, Y.; Bazuin, C. G.; Pézolet, M. *Macromolecules* **2001**, *34*, 6344−6352.
(33) Urban, V.; Panine, P.; Ponchut, C.; Boesecke, P.; Narayanan, T. *J. Appl. Crystallogr.* **2003**, *36*, 809−811.
(34) Fujimura, M.; Hashimoto, T.; Kawai, H. *Macromolecules* **1981**, *14*, 1309−1315.

(35) Alexander, L. E. *X-ray Diffraction Methods in Polymer Science*; Robert E. Krieger Publishing Co.: Huntington, NY, 1979.
(36) Gruger, A.; Régis, A.; Schmatko, T.; Colomban, P. *Vib. Spectrosc.* **2001**, *26*, 215−225.
(37) Yan, R. J.; Ajji, A.; Shinozaki, D. M. *J. Mater. Sci.* **1999**, *34*, 2335−2344.
(38) Matthews, R. G.; Ajji, A.; Dumoulin, M. M.; Prud'homme, R. E. *Polymer* **2000**, *41*, 7139−7145.
(39) Picken, S. J.; Aerts, J.; Doppert, H. L.; Reuvers, A. J.; Norholt, M. G. *Macromolecules* **1991**, *24*, 1366−1375.
(40) Hongladarom, K.; Burghardt, W. R.; Baek, S. G.; Cementwala, S.; Magda, J. J. *Macromolecules* **1993**, *26*, 772−784.
(41) Starkweather, H. W. J. *Macromolecules* **1982**, *15*, 320−323.
(42) De la Rosa, A.; Volino, F.; Blachot, J.-F.; Diat, O. To be submitted.
(43) Ludvigsson, M.; Lindgren, J.; Tegenfeldt, J. *J. Electrochem. Soc.* **2000**, *147*, 1303−1305.
(44) Porat, Z.; Fryer, J. R.; Huxham, M.; Rubinstein, I. *J. Phys. Chem.* **1995**, *99*, 4667−4671.
(45) Brandrup, J.; Immergut, E. H.; Grulke, E. A. *Polymer Handbook*; John Wiley & Sons: New York, 1999.
(46) Hiemenz, P. C. *Polymer Chemistry, The Basic Concepts*; Marcel Dekker: New York, 1984.

MA035642W